

Cotransport of Graphene Oxide Nanoparticles and Kaolinite Colloids in Porous Media

Constantinos V. Chrysikopoulos¹ ·
Nikolaos P. Sotirelis¹ · Nikolaos G. Kallithrakas-Kontos²

Received: 9 November 2016 / Accepted: 22 May 2017 / Published online: 13 June 2017
© Springer Science+Business Media Dordrecht 2017

Abstract This study examines the influence of pH and ionic strength (I_S) on the cotransport of graphene oxide (GO) nanoparticles and kaolinite (KGa-1b) colloids. Several flowthrough experiments were conducted in water-saturated columns, packed with either glass beads or quartz sand, in order to determine the transport behavior of GO and KGa-1b independently, as well as the cotransport behavior of GO together with KGa-1b. Various water chemistry conditions (pH = 4, 7, 10 and $I_S = 7, 12, 27$ mM) were considered. Collision efficiencies were calculated using the classical colloid filtration theory. Interaction energy profiles between GO nanoparticles or KGa-1b colloids and glass beads or quartz sand were constructed for the various experimental conditions, by using measured zeta potentials and applying the classical Derjaguin–Landau–Verwey–Overbeek theory. The cotransport experimental breakthrough data suggested that by lowering the pH, the retention of GO nanoparticles is enhanced, due to a possible increase in heteroaggregation between GO nanoparticles and KGa-1b colloids. Also, by increasing the I_S values, the retention of GO nanoparticles was slightly increased. The mass recovery of GO nanoparticles was reduced, and the transport of GO nanoparticles was retarded in the presence of KGa-1b colloids. Furthermore, the retention of GO nanoparticles was greater for columns packed with quartz sand than glass beads.

Keywords Graphene oxide · Kaolinite · Cotransport · Glass beads · Quartz sand · Porous media

List of Symbols

A_{123} Combined Hamaker constant, $M L^2/t^2$
 C_{GO} Concentration of GO nanoparticles, M/L^3

✉ Constantinos V. Chrysikopoulos
cvc@enveng.tuc.gr

¹ School of Environmental Engineering, Technical University of Crete, 73100 Chania, Greece

² School of Mineral Resources Engineering, Technical University of Crete, 73100 Chania, Greece

$C_{0(\text{GO})}$	Initial concentration of GO nanoparticles, M/L^3
C_i	Concentration of particles i , M/L^3
C_i^*	Concentration of particles i attached onto the solid matrix, M_i/M_s
$C_{0(i)}$	Initial concentration of particles i , M/L^3
$C_{\text{KGa-1b}}$	Concentration of KGa-1b colloids, M/L^3
$C_{0(\text{KGa-1b})}$	Initial concentration of KGa-1b colloids, M/L^3
d_c	Collector diameter, L
d_p	Colloidal particle diameter, L
e	Elementary charge (Coulomb), C
g	Acceleration due to gravity, L/t^2
h	Separation distance between two approaching surfaces, L
i	Subscript indicating the GO nanoparticles or KGa-1b colloids
I_S	Ionic strength (mol/L)
k_B	Boltzmann's constant, $\text{M L}^2/(\text{t}^2 \text{T})$
L	Length of packed column, L
M_n	n th normalized temporal moment, defined in Eq. (4), t^n
M_i	Mass of particles i , M_i
M_s	Mass of the solid matrix, M_s
$M_{\text{r}(i)}$	Mass recovery in the outflow of particles i (%)
$M_{\text{r}(\text{tr})}$	Tracer mass recovery in the outflow (%)
n	Subscript indicating the order of the moment (–)
N_A	Avogadro's number (1/mol)
r_{i-i^*}	Rate coefficient of particle attachment onto the solid matrix, $1/t$
r_{i^*-i}	Rate coefficient of particle detachment from the solid matrix, $1/t$
r_p	Colloidal particle radius, L
RB	Ratio of $M_{\text{r}(i)}$, relative to $M_{\text{r}(\text{tr})}$, (–)
t	Time, (t)
t_p	Time period of constant source concentration, t
T	Temperature in Kelvin, (T)
U	Pore water velocity, L/t
x	Cartesian coordinate, L

Greek Letters

α	Collision efficiency (–)
ε	Dielectric constant of the suspending liquid [$\text{C}^2/(\text{J m})$]
ε_r	Dimensionless relative dielectric constant of the suspending liquid (–)
ε_0	Permittivity of free space [$\text{C}^2/(\text{J m})$]
η_0	Dimensionless single-collector removal efficiency for favorable deposition (–)
θ	Porosity (–)
κ	Debye–Huckel length, $1/L$
μ_w	Absolute fluid viscosity, $\text{M}/(\text{L t})$
ρ_b	Dry bulk density, M/L^3
ρ_f	Fluid density, M/L^3
ρ_p	Particle density, M/L^3
Φ_{Born}	Born potential energy (J), $\text{M L}^2/\text{t}^2$
Φ_{dl}	Double layer potential energy (J), $\text{M L}^2/\text{t}^2$

$\Phi_{\max 1}$	Primary maximum of the total interaction energy (J), $\text{M L}^2/\text{t}^2$
$\Phi_{\min 1}$	Primary minimum of total interaction energy (J), $\text{M L}^2/\text{t}^2$
$\Phi_{\min 2}$	Secondary minimum of total interaction energy (J), $\text{M L}^2/\text{t}^2$
Φ_{vdW}	Van der Waals potential energy (J), $\text{M L}^2/\text{t}^2$
Ψ_1	Stern potential of GO nanoparticles (V)
Ψ_2	Stern potential of KGa-1b colloids (V)

1 Introduction

The fate and the transport of engineered nanoparticles in subsurface formations are of great importance because nanoparticles can adversely affect ecosystems and living beings (Liu and Cohen 2014). The transport of engineered nanoparticles is generally affected by the solution chemistry, type and size of materials comprising the porous medium, flow velocity, gravity effects, temperature, the presence of humic acid, biofilms, natural organic matter, and the presence of fine mineral particles (Jiang et al. 2013; Lanphere et al. 2013, 2014; Xiao and Wiesner 2013; Chrysikopoulos and Syngouna 2014; Kim and Lee 2014; Lv et al. 2014; Bayat et al. 2015; Cai et al. 2015; Sun et al. 2015).

Kaolinite (KGa-1b) is one of the most common minerals, which can be found in the subsurface (Wilson et al. 2014). Various experimental and theoretical studies have shown that kaolinite has a significant impact on the transport behavior of colloids, biocolloids (bacteria, viruses) and engineered nanoparticles (Vasiliadou and Chrysikopoulos 2011; Kim et al. 2012a,b; Cornelis et al. 2013; Syngouna and Chrysikopoulos 2013, 2016; Cai et al. 2014; Katzourakis and Chrysikopoulos 2014, 2015; Bayat et al. 2015). Therefore, the effects of the presence of suspended kaolinite particles on the transport of engineered nanomaterials in water-saturated porous media should be thoroughly understood.

Graphene oxide (GO) is a carbonaceous nanomaterial, which is used in many different applications, such as water purification/desalination, biomedical and electrochemical applications, photocatalysis, and biological or gas sensors (He et al. 2015; Hegab and Zou 2015; Reddy et al. 2015; Song et al. 2015; Tang et al. 2015; Toda et al. 2015). In addition, various studies have suggested that, under specific circumstances, GO can be toxic to plants, fish, mammalian organisms, and bacteria cells (Seabra et al. 2014; Chen et al. 2015; Hu et al. 2015; Liang et al. 2015; Wu et al. 2016). GO is a two-dimensional graphene-layered nanomaterial, composed of oxygen-bearing functional groups (Dreyer et al. 2010; Kim et al. 2012a). Therefore, GO sheets can be easily dispersed in water (Zhou et al. 2016). For these reasons, several investigators have studied how various factors (solution chemistry, initial concentration, grain size, unsaturated media, the presence of biofilm, heavy metals and surfactants) can influence the transport of GO in porous media (Feriancikova and Xu 2012; Lanphere et al. 2013; Liu et al. 2013, 2015; Fan et al. 2015a,b; Jian-Zhou et al. 2015; Sun et al. 2015; Zhou et al. 2016). Note that GO nanoparticles are expected to have a similar fate to carbon nanotubes, because of their similarities (e.g., nanometer size, carbon-based structure, and application in consumer electronic devices) (Lanphere et al. 2014). Also, approximately 80% of the carbon nanotubes manufactured will potentially end up in landfills (Keller et al. 2013). Therefore, it is almost certain that GO nanoparticles from landfills will easily migrate and pose a potential threat to underlying aquifers, where kaolinite is widely present (Han et al. 2008). Heteroaggregation of GO nanoparticles with kaolinite minerals is a critical process for the stability of GO nanoparticles (Wang et al. 2015), and the deposition of GO nanoparticles onto the solid matrix of subsurface formations can play a dominant role in the

cotransport of GO and KGa-1b. Recent studies suggested that the kinetics of GO nanoparticle attachment onto suspended kaolinite particles could be described with a pseudo-second-order model (Sotirelis and Chrysikopoulos 2017), which is associated with physicochemical interactions such as chemisorption (Ho 2006). However, to our knowledge, no previous work has examined the simultaneous transport (cotransport) of KGa-1b colloids with GO nanoparticles.

The scope of this work was to examine the cotransport of GO nanoparticles with KGa-1b colloids in water-saturated columns under various solution chemistry conditions and different types of porous media. Flowthrough experiments were performed in columns packed with either glass beads or quartz sand. Suspensions of GO, KGa-1b and GO–(KGa-1b), at three different pH values, and three different ionic strengths (I_s) were used. Appropriate collision efficiencies, mass recoveries and temporal moments were calculated. Furthermore, Derjaguin–Landau–Verwey–Overbeek (DLVO) energy profiles were constructed from the surface properties of GO or KGa-1b and glass beads or quartz sand, for the experimental conditions of this study.

2 Materials and Methods

2.1 Nanoparticles and Colloids

The GO sheets used in this study were purchased from Sigma-Aldrich (St. Louis, USA). A fresh GO suspension was prepared before each experiment by mixing appropriate mass of GO sheets with phosphate-buffered solution (PBS) at low ionic strength ($I_s = 7$ mM). The initial GO concentration, C_{GO} [M/L³], used for both transport and cotransport experiments was $C_{GO} = 5$ mg/L. The GO suspension was sonicated (Elmasonic S 30/(H), Elma Schmidbauer GmbH, Singen, Germany) for 2 h to ensure that the suspension was thoroughly uniform, as suggested by Sotirelis and Chrysikopoulos (2015, 2017).

Kaolinite (KGa-1b, well-crystallized kaolin, from Washington County, Georgia) (Pruett and Webb 1993), with specific surface area (SSA) of 10.1 m²/g, evaluated by the Brunauer–Emmett–Teller (BET) method, and cation exchange capacity (CEC) of 2.0 meq/100 g (van Olphen and Fripiat 1979) was purchased from Clay Minerals Society (Columbia, MO, USA). The desired <2 μm KGa-1b fraction was separated by sedimentation (Vasiliadou and Chrysikopoulos 2011) and was purified following the procedure described by Rong et al. (2008). A fresh KGa-1b suspension was prepared before each experiment by adding appropriate mass of KGa-1b colloids in phosphate-buffered solution (PBS) with low ionic strength ($I_s = 7$ mM). The initial KGa-1b concentration, C_{KGa-1b} [M/L³], used for both transport and cotransport experiments was $C_{KGa-1b} = 50$ mg/L.

All of the solutions were prepared with distilled deionized water (ddH₂O) with specific resistivity of ~18.2 MΩ · cm. The various GO and KGa-1b suspensions with different ionic strengths were adjusted with NaCl, whereas the suspensions with different pH values were adjusted with either H₂PO₄ or NaOH. Furthermore, all chemicals used in this study were of analytical reagent grade, employed without any additional purification.

The optical density of the GO nanoparticles and KGa-1b colloids was analyzed at wavelengths of 231 and 280 nm, respectively, by a UV–Visible spectrophotometer (Cary 400 BIO, Varian, Palo Alto, California). The corresponding concentrations of the GO nanoparticles and KGa-1b colloids were determined by the procedures outlined by Chrysikopoulos and Syngouna (2012), and Sotirelis and Chrysikopoulos (2015).

The effluent concentrations of the GO nanoparticles for the cotransport experiments were determined with the procedure outlined by [Zhao et al. \(2015\)](#). Each effluent liquid sample (2 mL) was centrifuged (3500 rpm or $1900 \times g$, 30 min), and then the optical density of the supernatant GO nanoparticles suspension was analyzed. Also, the KGa-1b colloids effluent concentrations for the cotransport experiments were determined with energy-dispersive X-ray fluorescence (EDXRF) (Spectro Xepos, AMETEK, USA), via detection of the aluminum (Al) present. The samples were analyzed directly by placing the effluent liquid in a special cup with a thin (4 mm) bottom layer of polymer Prolene (Chemplex) to reduce the X-ray absorption. Subsequently, each sample was irradiated for 900 s. All KGa-1b concentrations were determined by using a standard calibration curve of X-ray values (counts/s) versus KGa-1b concentration units (mg/L). It should be noted that for each measurement, the recorded X-ray (counts/s) were adjusted by subtracting the corresponding X-ray (counts/s) of a PBS sample in the absence of KGa-1b.

All zeta potentials and hydrodynamic diameter measurements for the GO nanoparticles and KGa-1b colloids, under the experimental conditions of this study, were measured in triplicate with a zetasizer (Nano ZS90, Malvern Instruments, Southborough, MA).

2.2 Packed Columns

The flowthrough experiments were conducted using glass columns with diameter of 2.5 cm and length of 30 cm. Each column was packed with either glass beads or quartz sand under standing PBS to minimize air entrapment. Screens at the inlet and outlet ends of the column held the glass beads in place and distributed the inflow evenly. The column was placed horizontally to reduce gravity effects ([Chrysikopoulos and Syngouna 2014](#)). For the column packed with glass beads, the estimated dry bulk density was determined as $\rho_b = 1.68 \pm 0.02 \text{ g/cm}^3$, the porosity $\theta = 0.42 \pm 0.01$, and the packed column pore volume $PV = 61.5 \pm 1.5 \text{ mL}$. Similarly, for the column packed with quartz sand, it was determined that $\rho_b = 1.70 \pm 0.02 \text{ g/cm}^3$, $\theta = 0.39 \pm 0.01$, and $PV = 56.7 \pm 1 \text{ mL}$.

Before each flowthrough experiment a fresh column was packed. The water-saturated packed column was equilibrated by injecting 2 PVs of the background solution, using a peristaltic pump (Masterflex L/S, Cole-Palmer). Subsequently, 3 PVs of the appropriate suspension (GO, KGa-1b or GO-KGa-1b) were injected, followed by 2 PVs of background solution. The flow rate (Darcian flux) was set to $q = 1.5 \text{ mL/min}$. All flowthrough experiments were conducted at room temperature ($\sim 25^\circ\text{C}$).

The column packings were either spherical glass beads with 2 mm diameter (Merck, Darmstadt, Germany) or quartz sand [(sieve no. 30), (96.2% SiO_2 , 0.15% Na_2O , 0.11% CaO , 0.02% MgO , 1.75% Al_2O_3 , 0.78% K_2O , 0.06% SO_3 , 0.46% Fe_2O_3 , 0.03% P_2O_5 , 0.02% BaO , 0.01% Mn_3O_4 , and 0.28% loss on ignition), (Filcom, Netherlands)]. The glass beads as well as the sand were carefully cleaned, following the procedures described by [Syngouna and Chrysikopoulos \(2013\)](#). Briefly, the packing materials were soaked in 0.1 M nitric acid HNO_3 (70%) for 3 h to remove surface impurities (e.g., metal hydroxides and organic coatings), rinsed with ddH_2O , then soaked in 0.1 M NaOH for 3 h, rinsed with ddH_2O again, then dried in an oven at 101°C , and finally stored in screw cap sterile beakers until use in the column experiments.

The zeta potentials of the two different column packings used in this study were determined and are listed in [Table 1](#). However, it should be noted that, because the glass beads and sand grains were too large for direct measurement by the zeta potential analyzer, a few glass beads and sand grains were crushed into fine powders and then mixed with the appropriate

Table 1 Measured zeta potentials

	Conditions		Zeta potential (mV)			
	pH	I_S (mM)	GO	KGa-1b	Glass beads	Quartz sand
$T = 25\text{ }^\circ\text{C}$, $C_{GO} = 5\text{ mg/L}$, $C_{KGa-1b} = 50\text{ mg/L}$, $C_{glass} = 200\text{ mg/L}$, $C_{sand} = 200\text{ mg/L}$	4	7	-24.3	-37.9	-35.1	–
	7	7	-36.2	-51.4	-54.1	-57.3
	10	7	-41.4	-54.2	-68.1	–
	7	12	-32.3	-49.7	-48.5	–
	7	27	-30.1	-46.7	-35.7	–

PBS solution to form a sufficiently stable suspension that could be used for zeta potential measurement (Stephan and Chase 2001; Mitropoulou et al. 2013).

Two sets of flowthrough experiments were performed. The first set of experiments was performed with GO nanoparticles, and KGa-1b colloids alone (transport experiments) in order to determine their individual transport behavior under various solution chemistry conditions. The second set of flowthrough experiments was performed to investigate the effect of the presence of KGa-1b colloids on GO nanoparticles transport (cotransport experiments) under various solution chemistry conditions. Both sets of experiments (transport and cotransport) were conducted at pH = 4, 7, 10 and $I_s = 7, 12, 27\text{ mM}$.

2.3 Tracer Tests

Chloride (Cl^-), in the form of 1 mM sodium chloride (NaCl) in ddH₂O, was chosen as the nonreactive tracer for the characterization of the packed column. It should be noted that alkali halides are the most commonly used salts for subsurface fluid tracing. The tracer experiments were performed by injecting 2 PVs of ddH₂O, followed by 3 PVs of tracer solution, followed by 2 PVs of ddH₂O. Effluent chloride concentrations were measured using ion chromatography (761 Compact IC, Metrohm, Switzerland).

3 Theoretical Considerations

3.1 Colloid Filtration Theory

The attachment behavior of GO nanoparticles and KGa-1b colloids onto glass beads and sand grains under the experimental conditions were explored with the classical colloid filtration theory. The dimensionless collision efficiency, $\alpha[-]$, which is the ratio of the collisions resulting in attachment to the total number of collisions between suspended particles and collector grains (Yao et al. 1971), was calculated from each breakthrough curve by the following expression (Rajagopalan and Tien 1976):

$$\alpha = -\frac{2d_c \ln(\text{RB})}{3(1-\theta)\eta_0 L} \quad (1)$$

where d_c [L] is the average collector diameter (2.0 and 0.7 mm, for glass beads and sand, respectively); η_0 [-] is the dimensionless single-collector removal efficiency for favorable deposition (in the absence of double layer interaction energy), which can be calculated from the relationship proposed by Tufenkji and Elimelech (2014); and RB is the ratio of suspended particles mass recovery relative to the tracer mass recovery, which was calculated by the following expression (Syngouna and Chrysikopoulos 2013):

Table 2 Measured hydrodynamic diameters

Conditions		Hydrodynamic diameter (nm)	
pH	I_S (mM)	GO	KGa-1b
4	7	552	662
7	7	524	635
10	7	413	513
7	12	598	657
7	27	654	709

$T = 25\text{ }^\circ\text{C}$, $C_{\text{GO}} = 5\text{ mg/L}$,
 $C_{\text{KGa-1b}} = 50\text{ mg/L}$

$$\text{RB} = \frac{M_{r(i)}}{M_{r(\text{tr})}} \quad (2)$$

where subscript “*i*” represents the type of suspended particles (GO or KGa-1b) and subscript “tr” the tracer; $M_{r(i)}$ [–] is the mass recovery of the suspended particles *i*; and $M_{r(\text{tr})}$ [–] is the tracer mass recovery in the outflow. The mass recovery of the suspended particles or the tracer was quantified by the following expression (Mitropoulou et al. 2013):

$$M_{r(i)}(L) = \frac{\int_0^{\infty} C_i(L, t) dt}{\int_0^{t_p} C_i(0, t) dt} \quad (3)$$

where t_p [t] is the time period of constant source concentration; C_i [M_i/L^3] is the concentration of suspended particles (subscript *i* represents GO nanoparticles or KGa-1b colloids); and *L* is the length of the packed column.

All theoretical α values for GO nanoparticles and KGa-1b colloids, for all transport and cotransport experiments, were calculated with Eq. (1) using the following parameter values: complex Hamaker constant, $A_{123} = 1.92 \times 10^{-21}$ [J] for GO–water–glass beads and GO–water–sand; $A_{123} = 7.04 \times 10^{-21}$ [J] for KGa-1b–water–(glass beads or sand); Boltzmann constant, $k_B = 1.38 \times 10^{-23}$ [J/K]; fluid absolute temperature, $T = 298$ K; particle diameters, d_p , of GO nanoparticles and KGa-1b colloids, listed in Table 2; particle density, $\rho_p = 2200\text{ kg/m}^3$ for GO nanoparticles (Stankovich et al. 2006); $\rho_p = 2650\text{ kg/m}^3$ for KGa-1b colloids (Haynes 2013); fluid density, $\rho_f = 999.7\text{ kg/m}^3$; absolute fluid viscosity, $\mu_w = 8.91 \times 10^{-4}\text{ kg/(m s)}$; and acceleration due to gravity, $g = 9.81\text{ m/s}^2$.

The factors expected to contribute to GO nanoparticle and KGa-1b colloid retention within the packed columns are straining, collector surface heterogeneity and angularity. However, in this work, straining cannot be considered as an important mechanism of mass loss, because the average size of the GO nanoparticles and KGa-1b colloids was approximately 0.05% and 0.14% of the average diameter of glass beads (2 mm) and sand (0.7 mm), respectively, which were much smaller than the 5% limit recommended by Hendry et al. (1999) and Choi et al. (2007), or the 0.5% limit recommended by Bradford et al. (2004).

3.2 Moment Analysis

The concentration breakthrough data obtained at the column exit, indicated as location $x=L$, were analyzed by the normalized temporal moments (Syngouna and Chrysikopoulos 2013):

$$M_n(x) = \frac{\int_0^\infty t^n C_i(x, t) dt}{\int_0^\infty C_i(x, t) dt} \tag{4}$$

The first normalized temporal moment, M_1 [t], defines the mean breakthrough time or average velocity. The second normalized temporal moment, M_2 [t^2], characterizes the temporal spreading of the breakthrough curve. Worthy to note is that the ratio $M_{1(i)}/M_{1(tr)}$ indicates the degree of velocity enhancement of colloid particle i relative to the conservative tracer. If this ratio is less than one, there exists nanoparticle or colloid retardation, and if it is greater than one, there exists velocity enhancement of nanoparticle or colloid transport (Syngouna and Chrysikopoulos 2013).

3.3 DLVO Theory

The interaction surface forces between GO nanoparticles and KGa-1b colloids with the glass beads and sand grains were calculated with the DLVO theory (Derjaguin and Landau 1941; Verwey and Overbeek 1948). According to the DLVO theory, the total energy interaction between two approaching surfaces Φ_{DLVO} [J] equals to the arithmetic sum of the van der Waals, Φ_{vdW} [J], double layer, Φ_{dl} [J], and Born, Φ_{Born} [J], potential energies (Loveland et al. 1996):

$$\Phi_{DLVO}(h) = \Phi_{vdW}(h) + \Phi_{dl}(h) + \Phi_{Born}(h) \tag{5}$$

here h [m] is the separation distance between the approaching surfaces.

Interaction energy profiles were constructed for all experimental conditions. It should be noted that a typical DLVO interaction energy profile is characterized by the primary minimum, Φ_{min1} (deep energy “well”), the primary maximum, Φ_{max1} (energy barrier to attachment and detachment), and the secondary minimum, Φ_{min2} (shallow energy “well”) (Chrysikopoulos and Syngouna 2012).

In this paper, the GO–glass beads, GO–sand, (KGa-1b)–glass beads and (KGa-1b)–sand interactions were treated as sphere–plate interactions because the sizes of the GO nanoparticles and KGa-1b colloids are much smaller compared to the size of glass beads or sand grains. Consequently, the Φ_{vdW} for the GO–glass beads, GO–sand, (KGa-1b)–glass beads and (KGa-1b)–sand interactions were calculated with the expression (Lyklema 1991; Voorn et al. 2007):

$$\Phi_{vdW}(h) = -\frac{A_{123}}{6} \left[\frac{2r_p(h+r_p)}{h(h+2r_p)} + \ln\left(\frac{h}{h+2r_p}\right) \right] \tag{6}$$

where r_p [L] is particle radius; and A_{123} [J] is the combined Hamaker constant for microscopic bodies of composition “1” and “3” in medium “2” [(1-GO or KGa-1b), (2-water), (3-glass or sand)] and can be estimated by the geometric mean combining rule (Yoon et al. 1997):

$$A_{123} = \sqrt{A_{121}A_{323}} \tag{7}$$

In this study, the combined Hamaker constants for the system GO–water–GO were set to $A_{121} = 2.23 \times 10^{-21}$ J (McAllister et al. 2007), for the system (KGa-1b)–water–(KGa-1b) was set to $A_{121} = 3.1 \times 10^{-20}$ J (Chrysikopoulos and Syngouna 2012) and for the system (glass or sand)–water–(glass or sand) was set to $A_{323} = 1.6 \times 10^{-21}$ (Ackler et al. 1996). Consequently, the A_{123} for (GO)–water–(glass or sand), (KGa-1b)–water–(glass or sand), and (GO)–water–(KGa-1b) were 1.89×10^{-21} J, 7.04×10^{-21} J, and 8.31×10^{-21} J,

respectively. Furthermore, the Φ_{dl} [J] for sphere–plate interactions were calculated with the expression (Voorn et al. 2007):

$$\Phi_{dl}(h) = \pi \epsilon_r \epsilon_0 r_p \left[(\Psi_1^2 + \Psi_2^2) \ln \left(\frac{\exp(2\kappa h) - 1}{\exp(2\kappa h)} \right) + 2\Psi_1\Psi_2 \ln \left(\frac{\exp(\kappa h) + 1}{\exp(\kappa h) - 1} \right) \right] \quad (8)$$

where Ψ_1 [V] is the Stern potential of the GO nanoparticle, Ψ_2 [V] is the Stern potential of the KGa-1b surface (in this study, we assumed that the Stern potential equals to zeta potential), and κ [1/m] is the inverse of the effective diffuse double layer thickness, known as the Debye–Huckel length:

$$\kappa = \left[\frac{2000 I_S N_A e^2}{\epsilon_r \epsilon_0 k_B T} \right]^{1/2} \quad (9)$$

where I_S [mol/L] is the ionic strength, $N_A = 6.02 \times 10^{23}$ [1/mol] is Avogadro’s number, and $e = 1.602 \times 10^{-19}$ [C] is the elementary charge; $\epsilon_r = \epsilon/\epsilon_0$ is the dimensionless relative dielectric constant of the suspending liquid, ϵ [C²/(J m)] is the dielectric constant of the suspending liquid, ϵ_0 [C²/(J m)] is the permittivity of free space, $k_B = 1.38 \times 10^{-23}$ [J/K] is the Boltzmann constant, and T [K] is the fluid absolute temperature.

The Φ_{Born} interactions forces were neglected because the Born potential energy is insignificant in aqueous systems. Also, the presence of hydrated ions is almost certain that will prevent surface–surface separation distances to diminish to the limiting value of $h \sim 0.3$ nm (Elimelech et al. 1995). In this paper, the interaction forces were intentionally calculated for $h > 0.3$ nm.

3.4 Transport Modeling

The transport of GO nanoparticles and KGa-1b colloids in one-dimensional water saturated, homogeneous porous media with uniform flow, accounting for nonequilibrium reversible attachment onto the solid matrix, is governed by the following partial differential equation (Sim and Chrysikopoulos 1995):

$$\frac{\partial C_i(t, x)}{\partial t} + \frac{\rho_b}{\theta} \frac{\partial C_i^*(t, x)}{\partial t} = -U \frac{\partial C_i(t, x)}{\partial x} + D_i \frac{\partial^2 C_i(t, x)}{\partial x^2} \quad (10)$$

where C_i [M_i/L³] is the concentration of suspended particles (subscript i is GO nanoparticles or KGa-1b colloids); C_i^* [M_i/M_s] is the concentration of particles attached onto the solid matrix (subscript i is GO nanoparticles or KGa-1b colloids); t [t] is time; x [L] is the Cartesian coordinate in the longitudinal direction; U [L/t] is the average interstitial velocity along the x-direction; and D_i [L²/t] is the longitudinal hydrodynamic dispersion coefficient of the suspended particles. The second accumulation term in Eq. (10) can be expressed as:

$$\frac{\rho_b}{\theta} \frac{\partial C_i^*(t, x)}{\partial t} = r_{i-i^*} C_i(t, x) - r_{i^*-i} C_i^*(t, x) \quad (11)$$

where r_{i-i^*} [1/t] is the rate coefficient of particle attachment onto the solid matrix, and r_{i^*-i} [1/t] is the rate coefficient of particle detachment from the solid matrix. The initial condition and the appropriate boundary conditions for a one-dimensional semi-infinite aquifer are as follows (Sim and Chrysikopoulos 1995):

$$C_i(0, x) = 0 \tag{12}$$

$$\frac{dC_i(t, \infty)}{dx} = 0 \tag{13}$$

$$-D_i \frac{\partial C_i(t, 0)}{\partial x} + UC_i(t, 0) = \begin{cases} UC_{0(i)}, & t \leq t_p \\ 0, & t > t_p \end{cases} \tag{14}$$

where $C_{0(i)}$ [M_i/L^3] is the injected constant concentration of particles. Condition (12) establishes that there is no initial particle concentration within the porous medium. The downstream condition (13) preserves concentration continuity. The flux-type boundary condition (14) for pulse injection, over a predefined time period t_p , implies concentration discontinuity at inlet and leads to material balance conservation (Chrysikopoulos et al. 1990). The analytical solution to the particle transport model (10) and (11), subject to conditions (12)–(14) has been developed by Sim and Chrysikopoulos (1995) as follows:

$$C_i(t, x) = \begin{cases} \Omega(t, x) & 0 < t \leq t_p \\ \Omega(t, x) - \Omega(t - t_p, x) & t > t_p \end{cases} \tag{15}$$

where

$$\begin{aligned} \Omega(t, x) = & \frac{C_{0(i)}U}{D_i^{1/2}} \exp\left[\frac{Ux}{2D_i}\right] \left\{ \int_0^t \int_0^\tau H e^{-H\tau} J_0[2(B\xi(\tau - \xi))^{1/2}] \right. \\ & \cdot \left\{ \frac{1}{(\pi\xi)^{1/2}} \exp\left[\frac{-x^2}{4D_i\xi} + \left(H - A - \frac{U^2}{4D_i}\right)\xi\right] \right. \\ & \left. \left. - \frac{U}{2D_i^{1/2}} \exp\left[\frac{Ux}{2D_i} + (H - A)\xi\right] \operatorname{erfc}\left[\frac{x}{2(D_i\xi)^{1/2}} + \frac{U}{2}\left(\frac{\xi}{D_i}\right)^{1/2}\right] \right\} d\xi d\tau \right. \\ & \left. + e^{-Ht} \int_0^t J_0[2(B\xi(t - \xi))^{1/2}] \right. \\ & \cdot \left\{ \frac{1}{(\pi\xi)^{1/2}} \exp\left[\frac{-x^2}{4D_i\xi} + \left(H - A - \frac{U^2}{4D_i}\right)\xi\right] \right. \\ & \left. \left. - \frac{U}{2D_i^{1/2}} \exp\left[\frac{Ux}{2D_i} + (H - A)\xi\right] \operatorname{erfc}\left[\frac{x}{2(D_i\xi)^{1/2}} + \frac{U}{2}\left(\frac{\xi}{D_i}\right)^{1/2}\right] \right\} d\xi \right\} \tag{16} \end{aligned}$$

where J_0 is the Bessel function of the first kind of zeroth order, “exp” is the exponential function; “erfc” is the complementary error function; ξ and τ are dummy integration variables; $A = r_{i-i^*}$; $B = r_{i-i^*}r_{i^*-i}\theta/\rho_b$; and $H = r_{i^*-i}\theta/\rho_b$ (Sim and Chrysikopoulos 1998). The above analytical solution is incorporated in the nonlinear least squares regression software ColloidFit (Katzourakis and Chrysikopoulos 2017) used in this study.

4 Results and Discussion

4.1 Transport Experiments

The experimental data from the tracer as well as the various GO nanoparticle transport experiments in columns packed with glass beads under different pH and I_S values are presented in

Fig. 1. Furthermore, the corresponding mass recoveries calculated with Eq. (3) are listed in Table 3. All tracer and GO nanoparticles breakthrough curves were nicely fitted with ColloidFit (Katzourakis and Chrysikopoulos 2017). Note that for $\text{pH} = 4$ and $I_S = 7$ (see Fig. 1b), the breakthrough data could not be fitted, because the simple transport model, Eq. (10), employed by ColloidFit does not account for the substantial GO aggregation that occurred under these conditions. As expected, the chloride tracer breakthrough curves yielded M_r values close to 100%, which suggested that there was no tracer retention by the packed column. Figure 1b–d shows the GO nanoparticles effluent concentrations for three different pH values ($\text{pH} = 4, 7, 10$). Note that for the case of $\text{pH} = 7$, there was only a slight retention of GO nanoparticles by the packed column ($M_r = 95.8\%$, see Table 3). For $\text{pH} = 4$, the mass recovery at the column exit ($M_r = 91.3\%$, see Table 3) was smaller than that at $\text{pH} = 7$, or equivalently the retention of GO nanoparticles was greater than that at $\text{pH} = 7$, whereas for $\text{pH} = 10$ no retention of GO nanoparticles was observed ($M_r = 100.4\%$, see Table 3). Clearly, decreasing the pH yielded smaller absolute zeta potential values (see Table 1), which resulted to smaller repulsion forces (Chen and Elimelech 2007) between GO nanoparticles, as well as between GO nanoparticles and glass beads. Similarly, Fig. 1f–h presents the effluent GO concentrations for three different I_S values ($I_S = 7, 12, 27$ mM). Based on the calculated M_r values listed in Table 3, it is evident that by increasing I_S the attachment of GO nanoparticles onto glass beads was enhanced, which led to greater retention by the packed column.

The experimental data from the tracer as well as the various KGa-1b colloid transport experiments in columns packed with glass beads under different pH and I_S values are presented in Fig. 2. Furthermore, the corresponding mass recoveries calculated with Eq. (3) are listed in Table 3. All tracer and KGa-1b colloid particles breakthrough curves were nicely fitted with ColloidFit (Katzourakis and Chrysikopoulos 2017). As expected, no tracer retention was observed, because both chloride tracer breakthrough curves yielded M_r values close to 100%. Figure 2b–d presents the KGa-1b colloid effluent concentrations for three different pH values ($\text{pH} = 4, 7, 10$). Note that for the case of $\text{pH} = 7$ (see Fig. 2c), there was significant retention of KGa-1b colloid particles by the packed column ($M_r = 76.6\%$, see Table 3). For $\text{pH} = 4$ values (see Fig. 2b), the KGa-1b mass recovery at the column exit was much smaller than the one observed at $\text{pH} = 7$ ($M_r = 48\%$, see Table 3) or equivalently the retention of KGa-1b colloids was quite larger than the one observed at $\text{pH} = 7$, probably due to the substantial aggregation of KGa-1b colloids at $\text{pH} = 4$ (Wang et al. 2015). Clearly, aggregation of KGa-1b colloids is expected to play a significant role on the transport and retention of KGa-1b colloids in water-saturated porous media. For $\text{pH} = 10$ (see Fig. 2d), a significant retention of KGa-1b colloids ($M_r = 72.5\%$, see Table 3) was observed. Note that the KGa-1b mass recovery at $\text{pH} = 10$ was slightly smaller ($M_r = 72.5\%$) than that observed at $\text{pH} = 7$ ($M_r = 76.6\%$). Similarly, Fig. 2f–h presents the effluent KGa-1b concentrations for three different I_S values ($I_S = 7, 12, 27$ mM). Based on the calculated M_r values listed in Table 3, it is evident that by increasing I_S the attachment of KGa-1b colloids onto glass beads was enhanced, which led to greater clay particle retention within the packed column. Worthy to note is that by increasing I_S , the absolute KGa-1b zeta potential values and the repulsion forces between KGa-1b colloids as well as between KGa-1b colloids and glass beads (or sand) were decreasing (see Table 1).

The experimental data from the tracer, GO nanoparticles, and KGa-1b colloids transport experiments in columns packed with quartz sand at $\text{pH} = 7$ and $I_S = 7$ mM are presented in Fig. 3. The corresponding mass recoveries calculated with Eq. (3) are listed in Table 3. The breakthrough curves were nicely fitted with ColloidFit. For all three cases (chloride tracer, GO nanoparticles, and KGa-1b colloids), the M_r values were smaller than the respective values

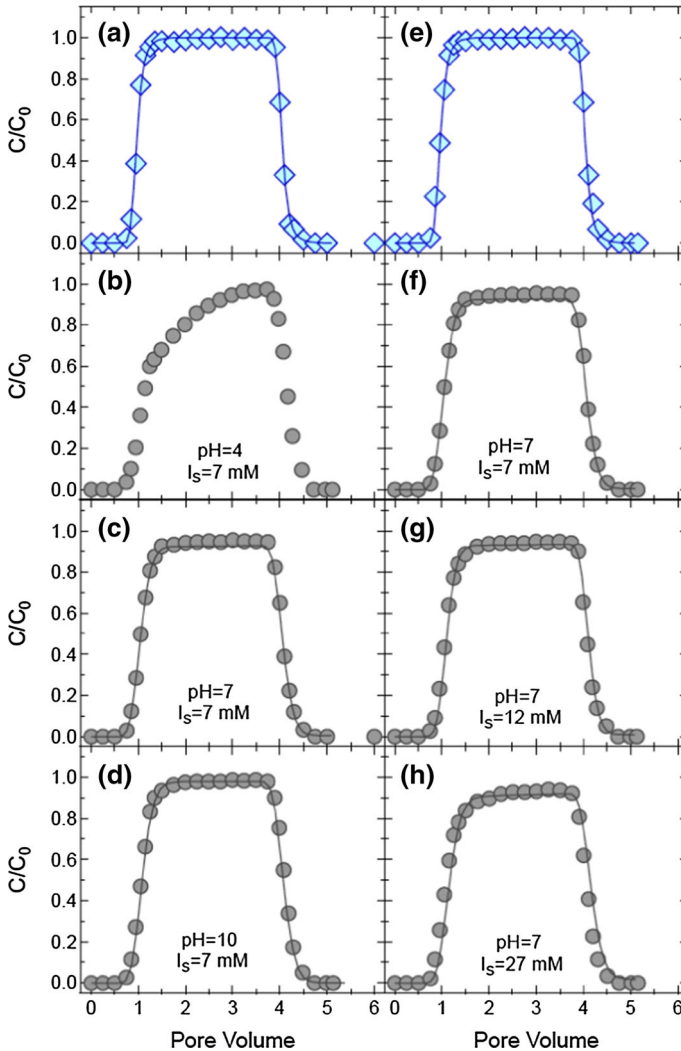


Fig. 1 Breakthrough data (symbols) and fitted model simulations (curves) for the transport of: **a, e** chloride (diamonds), and **b–d, f–h** GO nanoparticles (circles) in a column packed with glass beads, under various pH and I_s values (Here $T = 25^\circ\text{C}$, $C_{0(\text{Cl})} = 1\text{ mM}$, $C_{0(\text{GO})} = 5\text{ mg/L}$, $q = 1.5\text{ mL/min}$)

obtained from transport experiments in columns packed with glass beads (see Table 3). Also, the GO peak concentrations and mass recoveries were considerably higher than the KGa-1b peak concentrations (compare Fig. 3b, c, and M_r values in Table 3). This observation is in agreement with the results from the experiments with the column packed with glass beads (compare Fig. 1 with Fig. 2). The colloidal stability of GO nanoparticles is greater than KGa-1b colloids, because the critical coagulation concentration (CCC) is greater for GO nanoparticles than KGa-1b colloids, $\text{CCC}_{\text{GO}} > \text{CCC}_{\text{KGa-1b}}$ (Wu et al. 2013; Wang et al. 2015; Sotirelis and Chrysikopoulos 2017). Worthy to note is that, despite the fact that low M_r values cannot lead to the conclusion that the retained GO nanoparticles or KGa-1b colloids were irreversibly attached, the possibility that the observed low M_r values were caused by irreversible attachment cannot be ruled out.

Table 3 Estimated parameters associated with transport experiments

Conditions		GO			KGa-1b		
pH	I_S (mM)	M_r (%)	$M_{1(i)}/M_{1(tr)}$	α (-)	M_r (%)	$M_{1(i)}/M_{1(tr)}$	α (-)
<i>Glass beads</i>							
Tracer		102.1	1	—	103.2	1	—
Tracer		102.8	1	—	102.6	1	—
4	7	91.3	0.95	0.13	48.0	0.48	0.56
7	7	95.8	0.96	0.07	76.6	0.82	0.21
10	7	100.4	1.02	0.02	72.5	0.73	0.28
7	12	95.6	0.96	0.07	70.3	0.73	0.26
7	27	92.1	0.93	0.10	57.2	0.59	0.39
<i>Quartz sand</i>							
Tracer		93.8	1	—	—	—	—
7	7	78.6	0.84	0.04	64.6	0.71	0.07

The fitted parameters estimated by ColloidFit together with the corresponding 95% confidence intervals for the chloride tracer and all particle transport experiments are listed in Table 4. For the conservative tracer, only the dispersion coefficient was fitted. However, for the transport of GO nanoparticles and KGa-1b colloids, three parameters were fitted (D_i , r_{i-i^*} and r_{i^*-i}). Note that the fitted dispersion coefficient was smallest for the chloride tracer and largest for the bigger suspended particles (KGa-1b colloids). This observation is in perfect agreement with the work by Chrysikopoulos and Katzourakis (2015), who concluded that the dispersivity is particle size-dependent, and increases with increasing suspended particle size. Also, the dispersion coefficients for chloride, GO and KGa-1b were estimated to be greater for transport in columns packed with glass beads than quartz sand. In most of the cases considered, the attachment rate coefficients were greater for KGa-1b colloids than GO nanoparticles ($r_{K-K^*} > r_{G-G^*}$).

The collision efficiency values, α (-), were calculated with Eq. (1) for each transport experiment conducted with GO nanoparticles or KGa-1b colloids and are listed in Table 3. The calculated α values were greater for KGa-1b colloids than GO nanoparticles, which was in agreement with the observed smaller mass recovery of KGa-1b colloids. Also, the α values were greater for the transport experiments conducted in columns packed with glass beads than in columns packed with quartz sand. The greatest α values were determined at pH = 4, for both GO nanoparticles and KGa-1b colloids. Furthermore, the ratio $M_{1(i)}/M_{1(tr)}$ was computed for each transport experiment conducted with GO nanoparticles or KGa-1b colloids, and the values are listed in Table 3. Note that, for most of the cases considered $M_{1(i)}/M_{1(tr)} < 1$, indicating that the transport of GO nanoparticles and KGa-1b colloids was retarded compared to the conservative tracer.

4.2 Cotransport Experiments

For the cotransport experiments, only the suspended GO nanoparticle concentrations and the suspended total KGa-1b colloid concentrations were measured at the column exit. The total KGa-1b colloid concentrations represent the sum of the suspended KGa-1b colloids and the suspended GO-(KGa-1b) aggregates (GO nanoparticles attached onto KGa-1b colloids).

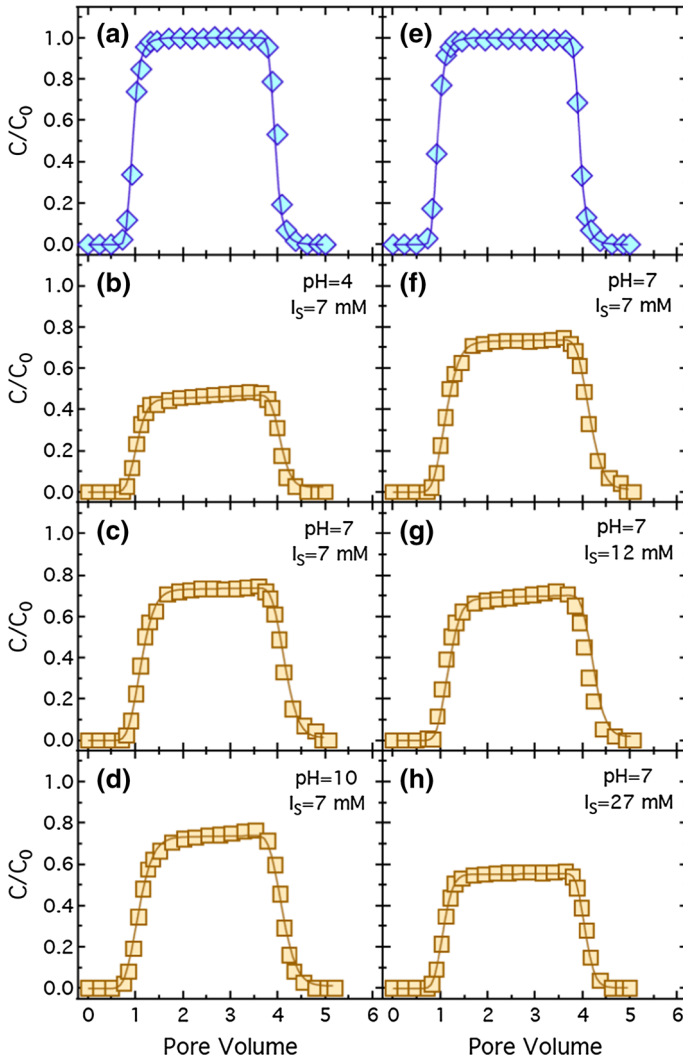
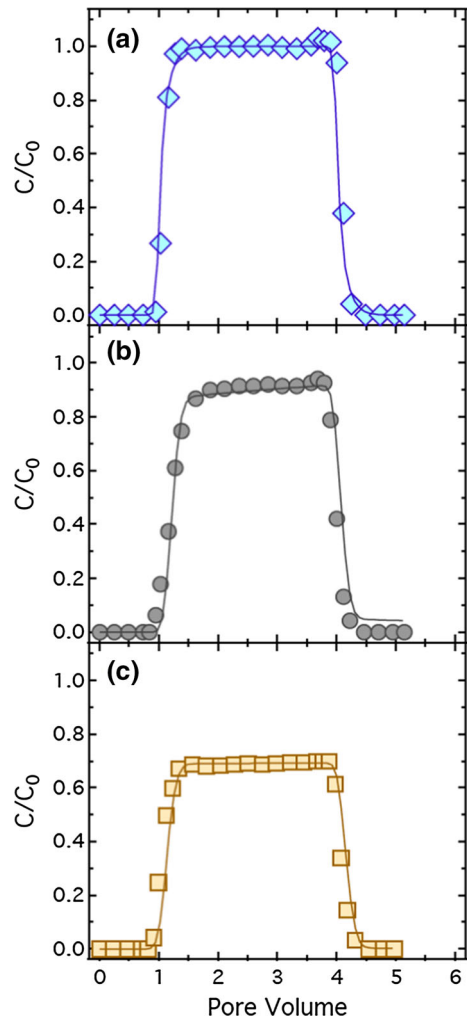


Fig. 2 Breakthrough data (symbols) and fitted model simulations (curves) for the transport of: **a, e** chloride (diamonds), and **b–d, f–h** KGa-1b colloids (squares) in a column packed with glass beads, under various pH and I_S values (Here $T = 25^\circ\text{C}$, $C_{0(\text{Cl})} = 1\text{ mM}$, $C_{0(\text{KGa-1b})} = 50\text{ mg/L}$, $q = 1.5\text{ mL/min}$)

In this study, the suspended KGa-1b colloids could not be differentiated from the GO–(KGa-1b) aggregates. Consequently, although advanced mathematical models for cotransport are available in the literature [Katzourakis and Chrysikopoulos \(2014, 2015\)](#), these models cannot be applied without experimental measurements of the required GO–(KGa-1b) effluent concentrations.

The effluent GO nanoparticle concentrations from the cotransport experiments conducted in columns packed with glass beads under different pH and I_S values are presented in Fig. 4. Furthermore, the corresponding mass recoveries calculated with Eq. (3) are listed in Table 5. Figure 4a–c presents the GO nanoparticle effluent concentrations for three different pH values (pH = 4, 7, 10). For pH = 7 and 10, the calculated mass recoveries $M_r = 92.7$ and 94.3% , respectively, indicated that there was a slight retention of GO nanoparticles by the packed

Fig. 3 Breakthrough data (symbols) and fitted model simulations (curves) for the transport of: **a** chloride, **b** GO nanoparticles, and **c** KGa-1b colloids in a column packed with quartz sand (Here $T = 25^\circ\text{C}$, $\text{pH} = 7$, $I_S = 7 \text{ mM}$, $C_0(\text{Cl}) = 1 \text{ mM}$, $C_0(\text{GO}) = 5 \text{ mg/L}$, $C_0(\text{KGa-1b}) = 50 \text{ mg/L}$, $q = 1.5 \text{ mL/min}$)



column. For low $\text{pH} = 4$, the retention of GO nanoparticles was substantial ($M_r = 53.8\%$, see Table 5). Figure 4d–f presents the GO nanoparticle effluent concentrations for three different I_S values ($I_S = 712, 27 \text{ mM}$). Based on the calculated M_r values listed in Table 5, it was evident that by increasing I_S , the attachment of GO nanoparticles onto glass beads was increased, which led to greater GO retention within the packed column. Worthy to note is that, the observed retention of GO nanoparticles by the packed column was greater for the cotransport than the transport experiments (compare M_r values in Tables 3, 5). Note that at $\text{pH} = 4$, the Al-O face/edge of KGa-1b colloids was positively charged (Wang et al. 2015). Consequently, at $\text{pH} = 4$ the attachment of the negatively charged GO nanoparticles onto KGa-1b colloids already attached onto the column packing material was more favorable. Furthermore, increasing I_S led to smaller absolute zeta potential values (see Table 1), which in turn led to smaller electric double layer repulsion between GO nanoparticles and KGa-1b colloids already attached onto the column packing material.

The effluent total KGa-1b colloid concentrations from the cotransport experiments conducted in columns packed with glass beads under different pH and I_S values are presented

Table 4 Fitted model parameters for transport experiments

Conditions		GO			KGa-Ib		
pH	I_s (mM)	D (cm ² /min)	r_{G-G^*} (1/m)	r_{G^*-G} (1/m)	D (cm ² /min)	r_{K-K^*} (1/m)	r_{K^*-K} (1/m)
<i>Glass beads</i>							
Tracer		0.15 ± 0.02	-	-	-	-	-
4	7	na	na	na	0.31 ± 0.09	0.019 ± 0.005	0.001 ± 0.000
7	7	0.32 ± 0.02	0.002 ± 0.000	0.001 ± 0.000	0.39 ± 0.06	0.007 ± 0.001	0.001 ± 0.000
10	7	0.30 ± 0.01	0.001 ± 0.00	0.001 ± 0.000	0.53 ± 0.15	0.007 ± 0.002	0.001 ± 0.000
7	12	0.23 ± 0.04	0.002 ± 0.000	0.001 ± 0.001	0.34 ± 0.07	0.008 ± 0.002	0.001 ± 0.000
7	27	0.38 ± 0.06	0.002 ± 0.001	0.002 ± 0.001	0.23 ± 0.05	0.014 ± 0.000	0.000 ± 0.000
<i>Quartz sand</i>							
Tracer		0.03 ± 0.00	-	-	-	-	-
7	7	0.10 ± 0.04	0.003 ± 0.001	0.005 ± 0.002	0.14 ± 0.02	0.009 ± 0.000	0.000 ± 0.000

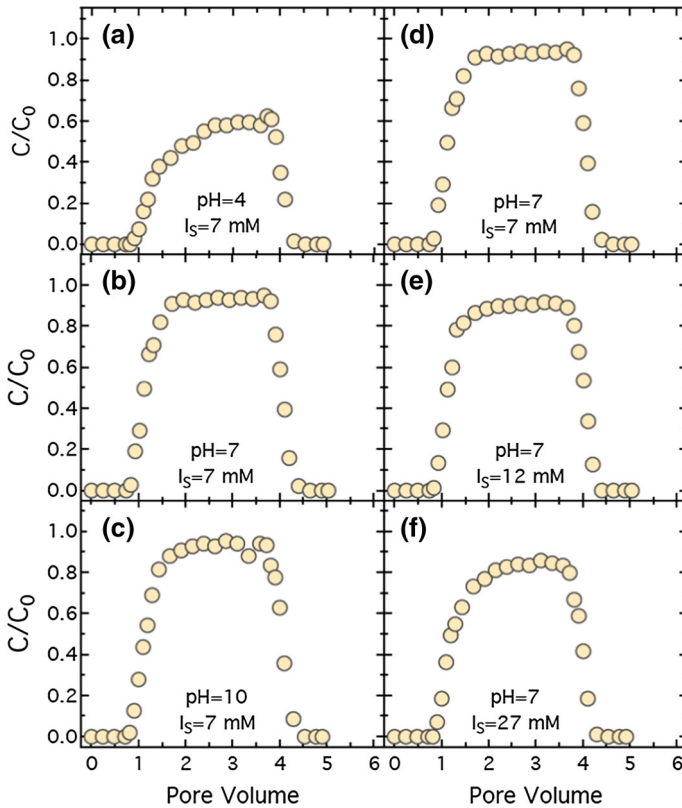


Fig. 4 Breakthrough data of GO nanoparticles from the cotransport experiments in a packed column with glass beads, under various pH and I_S values (Here $T = 25^\circ\text{C}$, $C_{0(\text{GO})} = 5 \text{ mg/L}$, $C_{0(\text{KGa-1b})} = 50 \text{ mg/L}$, $q = 1.5 \text{ mL/min}$)

in Fig. 5. The corresponding mass recoveries calculated with Eq. (3) are listed in Table 5. Figure 5a–c presents the KGa-1b colloid effluent concentrations for three different pH values (pH = 4, 7, 10), whereas Fig. 5d–f presents the effluent total KGa-1b colloid concentrations for three different I_S values ($I_S = 7, 12, 27 \text{ mM}$). The consistently low M_r values ($M_r < 22\%$, see Table 5) suggested that the total KGa-1b colloid mass retention by the packed column was very high for all cases considered. Also, the experimental data shown that decreasing pH or increasing I_S led to higher total KGa-1b colloid mass retention by the packed column.

The effluent GO nanoparticle and total KGa-1b colloid concentrations from the cotransport experiment in a column packed with quartz sand at pH = 7 and $I_S = 7 \text{ mM}$ are presented in Fig. 6. The corresponding mass recoveries calculated with Eq. (3) are listed in Table 5. Note that mass recovery was higher for GO ($M_r = 58.1\%$) than for total KGa-1b ($M_r = 12.9\%$). Furthermore, the calculated M_r values for both effluent concentrations (GO nanoparticles and total KGa-1b colloids) were greater for the column packed with glass beads than quartz sand (see Table 5).

The collision efficiency values, α (-), were calculated with Eq. (1) for each breakthrough curve of suspended GO nanoparticles and total KGa-1b colloids (see Table 5). The calculated α values were greater for the total KGa-1b colloids than GO nanoparticles. This result is consistent with the smaller M_r values determined for the total KGa-1b colloids. Also, the

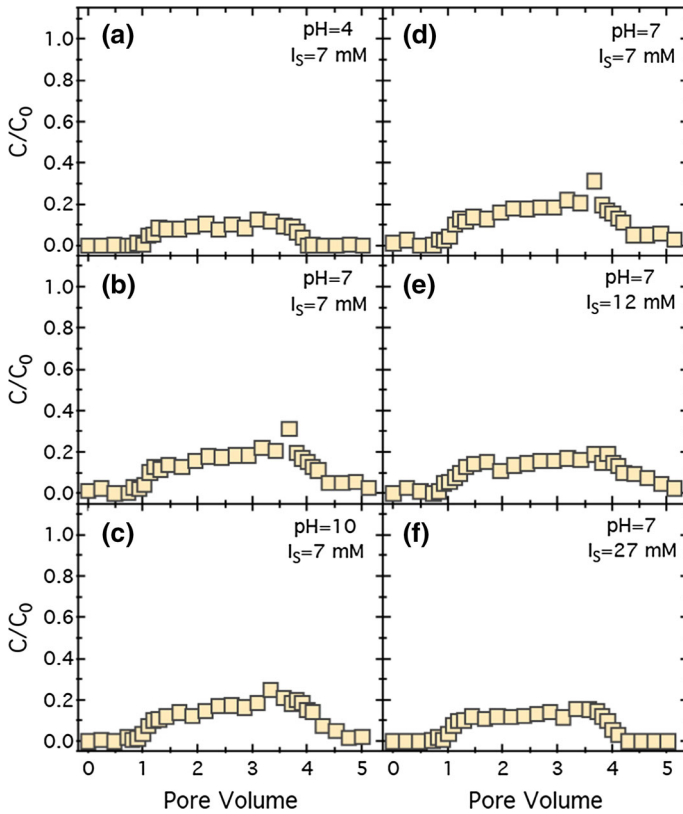


Fig. 5 Breakthrough data of the total KGa-1b colloids from the cotransport experiments in a packed column with glass beads, under various pH and I_S values (here $T = 25\text{ }^\circ\text{C}$, $C_{0(\text{GO})} = 5\text{ mg/L}$, $C_{0(\text{KGa-1b})} = 50\text{ mg/L}$, $q = 1.5\text{ mL/min}$)

calculated α values were greater for the experiments conducted in columns packed with glass beads than quartz sand. The greatest α values were determined at pH = 4, for both GO nanoparticles and total KGa-1b colloids. Furthermore, the ratio $M_{1(i)}/M_{1(\text{tr})}$ was computed for each effluent concentration collected from the cotransport experiments (see Table 5). Note that, for most of the cases considered, the calculated $M_{1(i)}/M_{1(\text{tr})} < 1$ values indicated that for the cotransport experiments, the GO nanoparticles and total KGa-1b colloids were retarded compared to the conservative chloride tracer. Worthy to note is that, for all cases considered, the RB values were smaller (more retardation) and the calculated α values were larger for the cotransport than the transport experiments.

4.3 DLVO Calculations

The effect of pH and I_S on the Φ_{DLVO} interaction energy profiles for GO–glass beads or (KGa-1b)–glass beads (sphere–plate model) is presented in Fig. 7. For pH = 7 and $I_S = 7\text{ mM}$, there is a shallow $\Phi_{\text{min}2}$ and a relatively high $\Phi_{\text{max}1}$, indicating the presence of strong repulsive forces between GO nanoparticles or KGa-1b colloids and glass beads. For pH = 4, there is a smaller $\Phi_{\text{max}1}$ and a deeper $\Phi_{\text{min}2}$ (see Fig. 7a, c). Furthermore, Fig. 7b, d illustrates the effect of I_S on the interaction energy profiles for GO–glass beads and (KGa-1b)–glass beads, respectively. Increasing I_S resulted in a small reduction in $\Phi_{\text{max}1}$ and considerable

Table 5 Estimated parameters associated with cotransport experiments

Conditions		GO			KGa-1b		
pH	I_S (mM)	M_r (%)	$M_{1(i)}/M_{1(tr)}$	$\alpha(-)$	M_r (%)	$M_{1(i)}/M_{1(tr)}$	$\alpha(-)$
<i>Glass beads</i>							
4	7	53.8	0.59	0.80	9.2	0.10	1.78
7	7	92.7	0.96	0.11	21.5	0.24	1.15
10	7	94.3	1.00	0.10	19.2	0.22	1.49
7	12	88.8	0.91	0.14	19.0	0.21	1.24
7	27	79.9	0.85	0.22	13.3	0.14	1.39
<i>Quartz sand</i>							
7	7	58.1	0.67	0.06	12.9	0.15	0.39

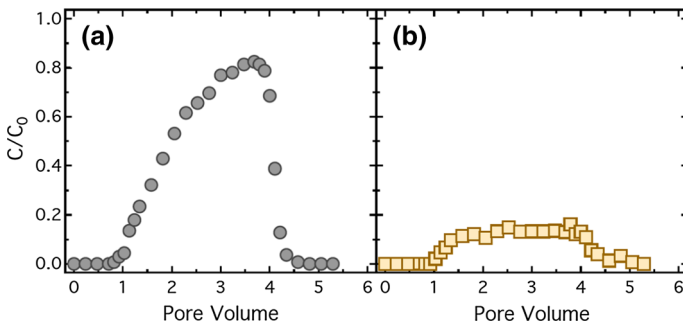


Fig. 6 Breakthrough data of: **a** GO nanoparticles, and **b** total KGa-1b colloids from the cotransport experiments in a packed column with quartz sand (Here $T = 25^\circ\text{C}$, $\text{pH} = 7$, $I_S = 7$ mM, $C_{0(\text{GO})} = 5$ mg/L, $C_{0(\text{KGa-1b})} = 50$ mg/L, $q = 1.5$ mL/min)

deepening in $\Phi_{\text{min}2}$ (see Fig. 7b, d). These findings are in agreement with the results from the transport and cotransport experiments of this study. Although the secondary energy minimum is deeper for $\text{pH} = 4$, $I_S = 27$ mM, the observed greater attachment of GO and KGa-1b onto glass beads and sand cannot be fully attributed to the deepening of $\Phi_{\text{min}2}$, because the energy barrier ($\Phi_{\text{max}1}$) is much greater than the secondary energy minimum ($\Phi_{\text{min}2}$). The interaction energy profiles between GO–sand or (KGa-1b)–sand (sphere–plate) for $\text{pH} = 7$ and $I_S = 7$ mM are presented in Fig. 8. Note that these energy profiles are very similar to the respective energy profiles for glass beads (compare Figs. 7 and 8).

5 Conclusions

The results of this study suggest that the presence of KGa-1b colloids, in columns packed with either glass beads or quartz sand, significantly affect the transport of GO nanoparticles. In all cases considered in this study, the M_r values of the suspended GO nanoparticles were lower in the presence of KGa-1b colloids. Furthermore, at $\text{pH} = 4$ and $I_S = 27$ mM, GO nanoparticles retention by the packed column was increased for both transport (absence of KGa-1b colloids) and cotransport experiments (presence of KGa-1b colloids). For all transport and cotransport experiments conducted, the migration of the suspended GO

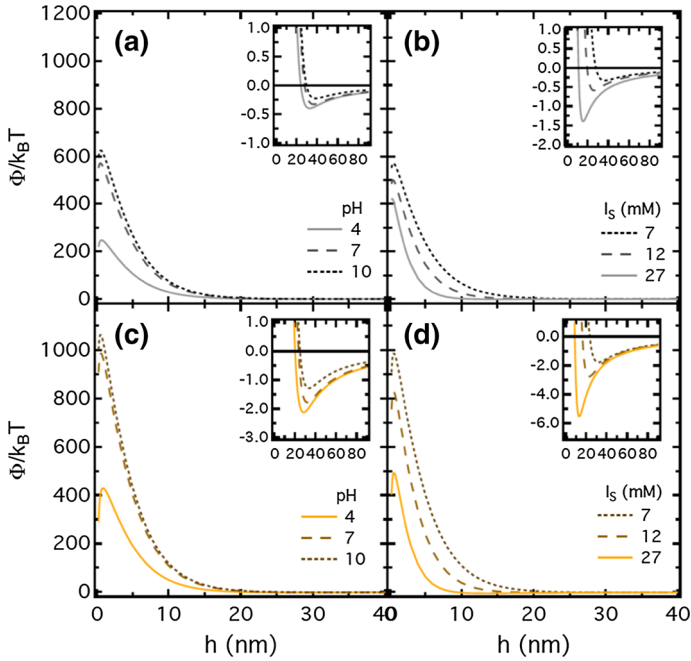


Fig. 7 Predicted DLVO total interaction energy profiles between: **a, b** GO–glass beads, and **c, d** (KGa-1b)–glass beads, as a function of separation distance for the experimental conditions. Each figure insert highlights the corresponding secondary energy minima

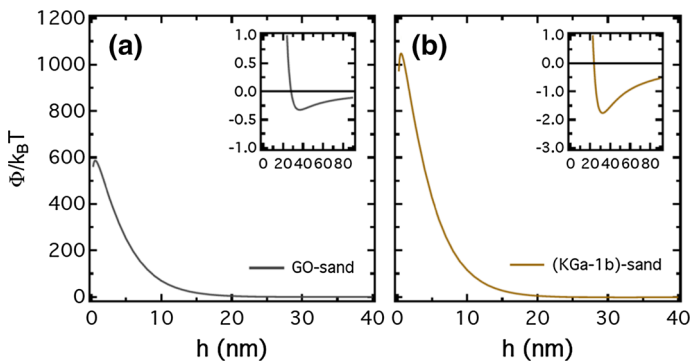


Fig. 8 Predicted DLVO total interaction energy profiles between: **a** GO–sand, and **b** (KGa-1b)–sand, as a function of separation distance for the experimental conditions. Each figure insert highlights the corresponding secondary energy minima. Here $\text{pH} = 7$ and $I_s = 7$ mM

nanoparticles was retarded ($M_{1(i)}/M_{1(\text{tr})} < 1$) compared to the chloride tracer. Also, GO nanoparticles were retained more by the quartz sand than the glass bead column packing in the presence and absence of KGa-1b colloids.

Acknowledgements The authors are thankful for the various suggestions and thoughtful comments provided by V.E. Katzourakis. This research did not receive any specific grant from funding agencies in the public, commercial, or not-for-profit sectors. NGK-K conducted the energy-dispersive X-ray fluorescence analysis.

References

- Ackler, H.D., French, R.H., Chiang, Y.M.: Comparisons of Hamaker constants for ceramic systems with intervening vacuum or water: from force laws and physical properties. *J. Colloid Interface Sci.* **179**, 460–469 (1996)
- Bayat, A.E., Junin, R., Mohsin, R., Hokmabadi, M., Shamshirband, S.: Influence of clay particles on Al₂O₃ and TiO₂ nanoparticles transport and retention through limestone porous media: measurements and mechanisms. *J. Nanopart. Res.* **17**(219), 1–14 (2015). doi:[10.1007/s11051-015-3031-4](https://doi.org/10.1007/s11051-015-3031-4)
- Bradford, S.A., Bettahar, M., Simunek, J., Genuchten, M.T.: Straining and attachment of colloids in physically heterogeneous porous media. *Vadose Zone J.* **3**, 384–394 (2004)
- Cai, L., Tong, M., Wang, X., Kim, H.: Influence of clay particles on the transport and retention of titanium dioxide nanoparticles in quartz sand. *Environ. Sci. Technol.* **48**(13), 7323–7332 (2014). doi:[10.1021/es5019652](https://doi.org/10.1021/es5019652)
- Cai, L., Zhu, J., Hou, Y., Tong, M., Kim, H.: Influence of gravity on transport and retention of representative engineered nanoparticles in quartz sand. *J. Contam. Hydrol.* **181**, 153–160 (2015)
- Chen, K.L., Elimelech, M.: Influence of humic acid on the aggregation kinetics of fullerene (C₆₀) nanoparticles in monovalent and divalent electrolyte solutions. *J. Colloid Interface Sci.* **309**(1), 126–134 (2007). doi:[10.1016/j.jcis.2007.01.074](https://doi.org/10.1016/j.jcis.2007.01.074)
- Chen, Y., Ren, C., Ouyang, S., Hu, X., Zhou, Q.: Mitigation in multiple effects of graphene oxide toxicity in Zebrafish embryogenesis driven by humic acid. *Environ. Sci. Technol.* **49**(16), 10147–10154 (2015). doi:[10.1021/acs.est.5b02220](https://doi.org/10.1021/acs.est.5b02220)
- Chrysikopoulos, C.V., Katzourakis, V.E.: Colloid particle size-dependent dispersivity. *Water Resour. Res.* **51**, 4668–4683 (2015). doi:[10.1002/2014WR016094](https://doi.org/10.1002/2014WR016094)
- Chrysikopoulos, C.V., Syngouna, V.I.: Attachment of bacteriophages MS2 and Φ X174 onto kaolinite and montmorillonite: extended-DLVO interactions. *Colloids Surf. B* **92**, 74–83 (2012). doi:[10.1016/j.colsurfb.2011.11.028](https://doi.org/10.1016/j.colsurfb.2011.11.028)
- Chrysikopoulos, C.V., Syngouna, V.I.: Effect of gravity on colloid transport through water-saturated columns packed with glass beads: modeling and experiments. *Environ. Sci. Technol.* **48**, 6805–6813 (2014). doi:[10.1021/es501295n](https://doi.org/10.1021/es501295n)
- Chrysikopoulos, C.V., Roberts, P.V., Kitanidis, P.K.: One-dimensional solute transport in porous media with partial well-to-well recirculation: application to field experiments. *Water Resour. Res.* **26**(6), 1189–1195 (1990)
- Choi, N.H., Kim, D.J., Kim, S.B.: Quantification of bacterial mass recovery as a function of pore-water velocity and ionic strength. *Res. Microbiol.* **158**, 70–78 (2007)
- Cornelis, G., Pang, L., Doolette, C., Kirby, J.K., McLaughlin, M.J.: Transport of silver nanoparticles in saturated columns of natural soils. *Sci. Total Environ.* **463–464**, 120–130 (2013). doi:[10.1016/j.scitotenv.2013.05.089](https://doi.org/10.1016/j.scitotenv.2013.05.089)
- Derjaguin, B.V., Landau, L.: Theory of the stability of strongly charged lyophobic sols and of the adhesion of strongly charged particles in solution of electrolytes. *Acta Physicochim. URSS* **14**, 633–662 (1941)
- Dreyer, D.R., Park, S., Bielawski, C.W., Ruoff, R.S.: The chemistry of graphene oxide. *Chem. Soc. Rev.* **39**, 228–240 (2010). doi:[10.1039/b917103g](https://doi.org/10.1039/b917103g)
- Elimelech, M., Gregory, J., Jia, X., Williams, R.A.: Particle Deposition & Aggregation: Measurement Modelling and Simulation. Butterworth-Heinemann Ltd, Oxford (1995)
- Fan, W., Jiang, X.H., Yang, W., Geng, Z., Huo, M.X., Liu, Z.M., Zhou, H.: Transport of graphene oxide in saturated porous media: effect of cation composition in mixed Na-Ca electrolyte systems. *Sci. Total Environ.* **511**, 509–515 (2015a). doi:[10.1016/j.scitotenv.2014.12.099](https://doi.org/10.1016/j.scitotenv.2014.12.099)
- Fan, W., Jiang, X.H., Lu, Y., Huo, M., Lin, S., Geng, Z.: Effects of surfactants on graphene oxide nanoparticles transport in saturated porous media. *J. Environ. Sci.* **35**, 12–19 (2015b). doi:[10.1016/j.jes.2015.02.007](https://doi.org/10.1016/j.jes.2015.02.007)
- Feriancikova, L., Xu, S.: Deposition and remobilization of oxide within saturated sand packs. *J. Hazard. Mater.* **235–236**, 194–200 (2012)
- Han, Z., Zhang, F., Lin, D., Xing, B.: Minerals affect the stability of surfactant-facilitated carbon nanotube suspensions. *Environ. Sci. Technol.* **42**, 6869–6875 (2008)
- Haynes, W.M. (ed.): CRC Handbook of Chemistry and Physics, 94th edn. CRC Press, Boca Raton (2013)
- He, C., Shi, Z.Q., Ma, L., Cheng, C., Nie, C.X., Zhou, M., Zhao, C.S.: Graphene oxide based heparin-mimicking and hemocompatible polymeric hydrogels for versatile biomedical applications. *J. Mater. Chem. B* **3**, 592–602 (2015). doi:[10.1039/C4TB01806K](https://doi.org/10.1039/C4TB01806K)
- Ho, Y.-S.: Review of second-order models for adsorption systems. *J. Hazard. Mater.* **136**(3), 681–689 (2006)
- Hegab, H.M., Zou, L.: Graphene oxide-assisted membranes: fabrication and potential applications in desalination and water purification. *J. Membr. Sci.* **484**, 95–106 (2015). doi:[10.1016/j.memsci.2015.03.011](https://doi.org/10.1016/j.memsci.2015.03.011)

- Hendry, M.J., Lawrence, J.R., Maloszewski, P.: Effect of velocity on the transport of two bacteria through saturated sand. *Ground Water* **37**, 103–112 (1999)
- Hu, C., Wang, Q., Zhao, H., Wang, L., Guo, S., Li, X.: Ecotoxicological effects of graphene oxide on protozoan *Euglena gracilis*. *Chemosphere* **128**, 184–190 (2015). doi:[10.1016/j.chemosphere.2015.01.040](https://doi.org/10.1016/j.chemosphere.2015.01.040)
- Jiang, X., Wang, X., Tong, M., Kim, H.: Initial transport and retention behaviors of ZnO nanoparticles in quartz sand porous media coated with *Escherichia coli* biofilm. *Environ. Pollut.* **174**, 38–49 (2013)
- Jian-Zhou, H., Cheng-Cheng, L., Deng-Jun, W., Zhou, D.M.: Biofilms and extracellular polymeric substances mediate the transport of graphene oxide nanoparticles in saturated porous media. *J. Hazard. Mater.* **300**, 467–474 (2015). doi:[10.1016/j.jhazmat.2015.07.026](https://doi.org/10.1016/j.jhazmat.2015.07.026)
- Katzourakis, V.E., Chrysikopoulos, C.V.: Mathematical modeling of colloid and virus cotransport in porous media. *Adv. Water Resour.* **68**, 62–73 (2014). doi:[10.1016/j.advwatres.2014.03.001](https://doi.org/10.1016/j.advwatres.2014.03.001)
- Katzourakis, V.E., Chrysikopoulos, C.V.: Modeling dense-colloid and virus cotransport in three-dimensional porous media. *J. Contam. Hydrol.* **181**, 102–113 (2015). doi:[10.1016/j.jconhyd.2015.05.010](https://doi.org/10.1016/j.jconhyd.2015.05.010)
- Katzourakis, V.E., Chrysikopoulos, C.V.: Fitting the transport and attachment of dense biocolloids in one-dimensional porous media: ColloidFit. *Groundwater* (2017). doi:[10.1111/gwat.12501](https://doi.org/10.1111/gwat.12501)
- Keller, A., McFerran, S., Lazareva, A., Suh, S.: Global life cycle releases of engineered nanomaterials. *J. Nanopart. Res.* **15**(6), 1–17 (2013). doi:[10.1007/s11051-013-1692-4](https://doi.org/10.1007/s11051-013-1692-4)
- Kim, H.J., Phenrat, T., Tilton, R.D., Lowry, G.V.: Effect of kaolinite, silica fines and pH on transport of polymer-modified zero valent iron nano-particles in heterogeneous porous media. *J. Colloid Interface Sci.* **370**, 1–10 (2012a). doi:[10.1016/j.jcis.2011.12.059](https://doi.org/10.1016/j.jcis.2011.12.059)
- Kim, J., Cote, L.J., Huang, J.: Two dimensional soft material: new faces of graphene oxide. *Acc. Chem. Res.* **45**(8), 1356–1364 (2012b). doi:[10.1021/ar300047s](https://doi.org/10.1021/ar300047s)
- Kim, C., Lee, S.: Effect of seepage velocity on the attachment efficiency of TiO₂ nanoparticles in porous media. *J. Hazard. Mater.* **279**, 163–168 (2014)
- Lanphere, J.D., Luth, C.J., Walker, S.L.: Effects of solution chemistry on the transport of graphene oxide in saturated porous media. *Environ. Sci. Technol.* **47**, 4255–4261 (2013)
- Lanphere, J.D., Rogers, B., Luth, C.J., Bolster, C.H., Walker, S.L.: Stability and transport of graphene oxide nanoparticles in groundwater and surface water. *Environ. Eng. Sci.* **31**(7), 350–359 (2014). doi:[10.1089/ees.2013.0392](https://doi.org/10.1089/ees.2013.0392)
- Liang, S., Xu, S., Zhang, D., He, J., Chu, M.: Reproductive toxicity of nanoscale graphene oxide in male mice. *Nanotoxicology* **9**(1), 92–105 (2015). doi:[10.3109/17435390.2014.893380](https://doi.org/10.3109/17435390.2014.893380)
- Liu, H.H., Cohen, Y.: Multimedia environmental distribution of engineered nanomaterials. *Environ. Sci. Technol.* **48**, 3281–3292 (2014). doi:[10.1021/es405132z](https://doi.org/10.1021/es405132z)
- Liu, L., Gao, B., Wu, L., Morales, V.L., Yang, L., Zhou, Z., Wang, H.: Deposition and transport of graphene oxide in saturated and unsaturated porous media. *Chem. Eng. J.* **229**, 444–449 (2013)
- Liu, L., Gao, B., Wu, L., Sun, Y., Zhou, Z.: Effects of surfactant type and concentration on graphene retention and transport in saturated porous media. *Chem. Eng. J.* **262**, 1187–1191 (2015). doi:[10.1016/j.ccej.2014.10.032](https://doi.org/10.1016/j.ccej.2014.10.032)
- Loveland, J.P., Ryan, J.N., Amy, G.L., Harvey, R.W.: The reversibility of virus attachment to mineral surfaces. *Colloids Surf. A* **107**, 205–221 (1996)
- Lv, X., Gao, B., Sun, Y., Shi, X., Xu, H., Wu, J.: Effects of humic acid and solution chemistry on the retention and transport of cerium dioxide nanoparticles in saturated porous media. *Water Air Soil Pollut.* **225**, 2167 (2014). doi:[10.1007/s11270-014-2167-7](https://doi.org/10.1007/s11270-014-2167-7)
- Lyklema, J.: *Fundamentals of Interface and Colloid Science*. Academic Press, London (1991)
- Mitropoulou, P.N., Syngouna, V.I., Chrysikopoulos, C.V.: Transport of colloids in unsaturated packed columns: role of ionic strength and sand grain size. *Chem. Eng. J.* **232**, 237–248 (2013)
- Pruett, R.J., Webb, H.L.: Sampling and analysis of KGa-1b well-crystallized kaolin source clay. *Clays. Clay. Miner.* **41**(4), 514–519 (1993)
- Rajagopalan, R., Tien, C.: Trajectory analysis of deep-bed filtration with the sphere-in-cell porous media model. *AIChE J.* **22**, 523–533 (1976)
- Reddy, D.A., Ma, R., Choi, M.Y., Kim, T.K.: Reduced graphene oxide wrapped ZnS–Ag₂S ternary composites synthesized via hydrothermal method: Applications in photocatalyst degradation of organic pollutants. *Appl. Surf. Sci.* **324**, 725–735 (2015). doi:[10.1016/j.apsusc.2014.11.026](https://doi.org/10.1016/j.apsusc.2014.11.026)
- Rong, X., Huang, Q., He, X., Chen, H., Cai, P., Liang, W.: Interaction of *Pseudomonas putida* with kaolinite and montmorillonite: a combination study by equilibrium adsorption, ITC, SEM and FTIR. *Colloids Surf. B* **64**, 49–55 (2008)
- Seabra, A.B., Paula, A.J., de Lima, R., Alves, O.L., Durán, N.: Nanotoxicity of graphene and graphene oxide. *Chem. Res. Toxicol.* **27**(2), 159–168 (2014). doi:[10.1021/tx400385x](https://doi.org/10.1021/tx400385x)
- Sim, Y., Chrysikopoulos, C.V.: Analytical models for one-dimensional virus transport in saturated porous media. *Water Resour. Res.* **31**(5), 1429–1437 (1995). doi:[10.1029/95WR00199](https://doi.org/10.1029/95WR00199)

- Sim, Y., Chrysikopoulos, C.V.: Three-dimensional analytical models for virus transport in saturated porous media. *Transp. Porous Med.* **30**, 87–112 (1998). doi:[10.1023/A:1006596412177](https://doi.org/10.1023/A:1006596412177)
- Song, Z., Wang, X., Zhu, G., Nian, Q., Zhou, H., Yang, D., Qin, C., Tang, R.: Virus capture and destruction by label-free graphene oxide for detection and disinfection applications. *Small* **11**(9–10), 1171–1176 (2015). doi:[10.1002/sml.201401706](https://doi.org/10.1002/sml.201401706)
- Sotirelis, N.P., Chrysikopoulos, C.V.: Interaction between graphene oxide nanoparticles and quartz sand. *Environ. Sci. Technol.* **94**(22), 13413–13421 (2015). doi:[10.1021/acs.est.5b03496](https://doi.org/10.1021/acs.est.5b03496)
- Sotirelis, N.P., Chrysikopoulos, C.V.: Heteroaggregation of graphene oxide nanoparticles and kaolinite colloids. *Sci. Total Environ.* **579**, 736–744 (2017). doi:[10.1016/j.scitotenv.2016.11.034](https://doi.org/10.1016/j.scitotenv.2016.11.034)
- Stankovich, S., Dikin, D.A., Dommett, G.H., Kohlhaas, K.M., Zimney, E.J., Stach, E.A., Piner, R.D., Nguyen, S.T., Ruoff, R.S.: Graphene-based composite materials. *Nature* **442**, 282–285 (2006). doi:[10.1038/nature04969](https://doi.org/10.1038/nature04969)
- Stephan, E.A., Chase, G.G.: A preliminary examination of zeta potential and deep bed filtration activity. *Sep. Purif. Technol.* **21**, 219–226 (2001)
- Sun, Y., Gao, B., Bradford, S.A., Wu, L., Chen, H.: Transport, retention, and size perturbation of graphene oxide in saturated porous media: effects of input concentration and grain size. *Water Res.* **68**, 24–33 (2015). doi:[10.1016/j.watres.2014.09.025](https://doi.org/10.1016/j.watres.2014.09.025)
- Syngouna, V.I., Chrysikopoulos, C.V.: Cotransport of clay colloids and viruses in water saturated porous media. *Colloids Surf. A.* **416**, 56–65 (2013). doi:[10.1016/j.colsurfa.2012.10.018](https://doi.org/10.1016/j.colsurfa.2012.10.018)
- Syngouna, V.I., Chrysikopoulos, C.V.: Cotransport of clay colloids and viruses through water-saturated vertically oriented columns packed with glass beads: gravity effects. *Sci. Total Environ.* **545–546**, 210–218 (2016). doi:[10.1016/j.scitotenv.2015.12.091](https://doi.org/10.1016/j.scitotenv.2015.12.091)
- Tang, H., Zhang, J., Zhang, Y.J., Xiong, Q.Q., Tong, Y.Y., Li, Y., Wang, X.L., Gu, C.D., Tu, J.P.: Porous reduced graphene oxide sheet wrapped silicon composite fabricated by steam etching for lithium-ion battery application. *J. Power Sources* **286**, 431–437 (2015). doi:[10.1016/j.jpowsour.2015.03.185](https://doi.org/10.1016/j.jpowsour.2015.03.185)
- Toda, K., Furue, R., Hayami, S.: Recent progress in applications of graphene oxide for gas sensing: a review. *Anal. Chim. Acta.* **878**, 43–53 (2015). doi:[10.1016/j.aca.2015.02.002](https://doi.org/10.1016/j.aca.2015.02.002)
- Tufenkji, N., Elimelech, M.: Correlation equation for predicting single-collector efficiency in physicochemical filtration in saturated porous media. *Environ. Sci. Technol.* **38**(2), 529–536 (2014). doi:[10.1021/es034049r](https://doi.org/10.1021/es034049r)
- van Olphen, H., Fripiat, J.J.: *Data Handbook for Clay Minerals and Other Non-metallic Minerals*. Pergamon Press, Oxford (1979)
- Vasiliadou, I.A., Chrysikopoulos, C.V.: Cotransport of *Pseudomonas putida* and kaolinite particles through water saturated columns packed with glass beads. *Water Resour. Res.* **47**(2), W02543 (2011). doi:[10.1029/2010WR009560](https://doi.org/10.1029/2010WR009560)
- Verwey, E.J.W., Overbeek, J.T.G.: *Theory of the Stability of Lyophobic Colloids*, p. 205. Elsevier, Amsterdam (1948)
- Voorn, D.J., Ming, W., Laven, J., Meuldijk, J., de With, G., van Herk, A.M.: Plate-sphere hybrid dispersions: heterocoagulation kinetics and DLVO evaluation. *Colloids Surf. A.* **294**(1–3), 236–246 (2007). doi:[10.1016/j.colsurfa.2006.08.022](https://doi.org/10.1016/j.colsurfa.2006.08.022)
- Wang, H., Dong, Y.N., Zhu, M., Li, X., Keller, A.A., Wang, T., Li, F.: Heteroaggregation of engineered nanoparticles and kaolin clays in aqueous environments. *Water Res.* **80**, 130–138 (2015). doi:[10.1016/j.watres.2015.05.023](https://doi.org/10.1016/j.watres.2015.05.023)
- Wilson, M.J., Wilson, L., Patey, I.: The influence of individual clay minerals on formation damage of reservoir sandstones: a critical review with some new insights. *Clay Miner.* **49**(2), 147–164 (2014). doi:[10.1180/claymin.2014.049.2.02](https://doi.org/10.1180/claymin.2014.049.2.02)
- Wu, L., Liu, L., Gao, B., Muñoz-Carpena, R., Zhang, M., Chen, H., Zhou, Z., Wang, H.: Aggregation kinetics of graphene oxides in aqueous solutions: experiments, mechanisms, and modeling. *Langmuir* **29**, 15174–15181 (2013)
- Wu, W., Yan, L., Wu, Q., Li, Y., Li, Q., Chen, S., Yang, Y., Gu, Z., Xu, H., Yin, Z.Q.: Evaluation of the toxicity of graphene oxide exposure to the eye. *Nanotoxicology* **10**(9), 1329–1340 (2016). doi:[10.1080/17435390.2016.1210692](https://doi.org/10.1080/17435390.2016.1210692)
- Xiao, Y., Wiesner, M.R.: Transport and retention of selected engineered nanoparticles by porous media in the presence of a biofilm. *Environ. Sci. Technol.* **47**(5), 2246–2253 (2013). doi:[10.1021/es304501n](https://doi.org/10.1021/es304501n)
- Yao, K.M., Habibian, M.T., O'Melia, C.R.: *Water and waste water filtration. Concepts and Applications*. Environ. Sci. Technol. **5**(11), 1105–1112 (1971). doi:[10.1021/es60058a005](https://doi.org/10.1021/es60058a005)
- Yoon, R.-H., Flin, D.H., Rabinovich, Y.I.: Hydrophobic interactions between dissimilar surfaces. *J. Colloid Interface Sci.* **185**, 363–370 (1997)

- Zhao, J., Liu, F., Wang, Z., Cao, X., Xing, B.: Heteroaggregation of graphene oxide with minerals in aqueous phase. *Environ. Sci. Technol.* **49**(5), 2849–2857 (2015). doi:[10.1021/es505605w](https://doi.org/10.1021/es505605w)
- Zhou, D.D., Jiang, X.H., Lub, Y., Fan, W., Huo, M.X., Crittenden, J.C.: Cotransport of graphene oxide and Cu(II) through saturated porous media. *Sci. Total Environ.* **550**, 717–726 (2016). doi:[10.1016/j.scitotenv.2016.01.141](https://doi.org/10.1016/j.scitotenv.2016.01.141)